

# First order shape transition and critical point nuclei in Sm isotopes from relativistic mean field approach

J. Meng,<sup>1,2,3,\*</sup> W. Zhang,<sup>1</sup> S.-G. Zhou,<sup>1,4,2,3</sup> H. Toki,<sup>5</sup> and L.S. Geng<sup>1,5</sup>

<sup>1</sup>*School of Physics, Peking University, Beijing 100871, China*

<sup>2</sup>*Institute of Theoretical Physics, Chinese Academy of Sciences, Beijing 100080, China*

<sup>3</sup>*Center of Theoretical Nuclear Physics, National Laboratory of Heavy Ion Accelerator, Lanzhou 730000, China*

<sup>4</sup>*Max-Planck-Institut für Kernphysik, 69029 Heidelberg, Germany*

<sup>5</sup>*Research Center for Nuclear Physics (RCNP), Osaka University, Ibaraki, Osaka 567-0047, Japan*  
(Dated: August 1, 2017)

The critical point nuclei in Sm isotopes, which marks the first order phase transition between spherical U(5) and axially deformed shapes SU(3), have been investigated in the microscopic quadrupole constrained relativistic mean field (RMF) model plus BCS method with all the most used interactions, i.e., NL1, NL3, NLSH and TM1. The calculated potential energy surfaces show a clear shape transition for the even-even Sm isotopes with  $N = 82 \sim 96$  and the critical point nuclei are found to be  $^{148}\text{Sm}$ ,  $^{150}\text{Sm}$  and  $^{152}\text{Sm}$ . Similar conclusions can also be drawn from the microscopic neutron and proton single particle spectra.

PACS numbers: 21.10-k, 21.60.Jz, 21.60.Fw, 21.10.Re

The equilibrium shape for finite many-body systems such as nucleus, atom, molecule, etc. have been a hot topic for the past several decades. These shapes are normally not rigid and change as a function of their constituents. Sometimes these changes can be quite abrupt and exhibit phase transitional and critical point behavior similar to that found in a wide variety of many-body systems, though the concepts of phase transitions are only approximate for finite system.

Properties of the system in the transition region and, in particular, at the critical point can be found by solving numerically the eigenvalue problem for the Hamiltonian. However, the transition regions are difficult to interpret as they exhibit a complicated interplay of competing degrees of freedom. Yet such system are in many respects the most important, as their structure defines the nature of the transition region itself.

Recently, the concept of such critical point solutions has been introduced in the framework of the algebraic models, in which different shapes (phases) correspond to dynamic symmetries of some algebraic structure  $G$  and the phase transition corresponds to the breaking of the dynamical symmetries. In the Interacting Boson Model [1]  $G \equiv \text{U}(6)$  and there are three dynamical symmetries characterized by the first algebra in the chain originating from U(6), that is U(5), SU(3), and SO(6), with spherical, axially deformed, and  $\gamma$ -unstable shapes. Experimental examples of all three types of symmetries can be found in nuclei, e.g., the U(5) nuclei can occur near closed shells, SU(3) nuclei can occur in the middle of shells, and the O(6) limit tends to occur in nuclei with particles-holes configuration. The phase transition between spherical U(5) and axially deformed shapes SU(3) is first order [2, 3]. The phase/shape transition region is characterized by a pronounced  $\beta$  softness [4]. This characteristic led to the analytic solution for critical

point nuclei, called X(5) for axially symmetric case, and is based on analytic solutions of the Schrödinger equation corresponding to a geometric (Bohr) Hamiltonian with a square-well potential [5]. It has been shown that  $^{152}\text{Sm}$  [6] and other  $N = 90$  isotones [7] are the first empirical manifestation of the predicted nuclei at the critical point of vibrator (spherical shape) to axial rotor (axially deformed shape) phase transition.

The critical-point symmetries provide a classification of states and analytic expressions for observables in regions where the structure changes most rapidly. The ideas can be visualized in terms of two coexisting potentials, spherical and deformed, whose energy separation varies with nucleon number. Although phase transitions and critical point have been discussed in atomic nuclei for many years, there is no microscopical investigations yet. As an important complementary way, a microscopical study could be very helpful for us to understand where and how nuclei exhibiting structures close to these symmetries occur. It is the main purpose of this Letter to close this gap in the study of symmetry. The relativistic mean field (RMF) theory [8] has received wide attention because of its successful description of many nuclear phenomena during the past years [9]. In particular, the exotic halo phenomena can be understood self-consistently in this microscopical model after the proper treatment of the continuum effect [10, 11, 12]. Here in this letter we will discuss the realization of the critical point concept in atomic nuclei in the microscopic quadrupole constrained RMF theory with pairing treated by the BCS method, which will show that  $^{148,150,152}\text{Sm}$  are excellent empirical manifestations of this critical point structure.

The basic Ansatz of the RMF theory is a Lagrangian density where nucleons are described as Dirac particles which interact via the exchange of various mesons including the isoscalar-scalar  $\sigma$  meson, the isoscalar-vector

TABLE I: The total binding energy and the quadrupole deformation  $\beta_2$  of the ground-states of  $^{144-158}\text{Sm}$  calculated by the constrained RMF theory with the parameter sets NL1, NL3, NLSH and TM1.

$E[\text{MeV}]$	EXP <sup>[20]</sup>	NL1	NL3	NLSH	TM1
$^{144}\text{Sm}$	1195.74	1201.28	1198.34	1200.20	1201.63
$^{146}\text{Sm}$	1210.91	1213.83	1211.79	1214.00	1215.89
$^{148}\text{Sm}$	1225.40	1225.95	1225.48	1227.95	1230.12
$^{150}\text{Sm}$	1239.25	1239.59	1239.29	1241.09	1243.54
$^{152}\text{Sm}$	1253.11	1252.78	1253.54	1255.39	1256.12
$^{154}\text{Sm}$	1266.94	1265.50	1267.54	1269.59	1268.99
$^{156}\text{Sm}$	1279.99	1276.98	1280.05	1282.26	1281.61
$^{158}\text{Sm}$	1291.98	1287.57	1291.73	1293.99	1293.07
$\beta_2$	EXP <sup>[21]</sup>	NL1	NL3	NLSH	TM1
$^{144}\text{Sm}$	0.00	0.00	0.00	-0.01	0.00
$^{146}\text{Sm}$	0.00	0.05	0.06	0.08	0.06
$^{148}\text{Sm}$	0.16	0.15	0.14	0.14	0.13
$^{150}\text{Sm}$	0.21	0.25	0.23	0.21	0.16
$^{152}\text{Sm}$	0.24	0.34	0.30	0.28	0.19
$^{154}\text{Sm}$	0.27	0.35	0.33	0.32	0.31
$^{156}\text{Sm}$	0.28	0.36	0.34	0.33	0.33
$^{158}\text{Sm}$	0.28	0.36	0.35	0.34	0.34

$\omega$  meson and the isovector-vector  $\rho$  meson. The effective Lagrangian density considered is written in the form:

$$\begin{aligned}
\mathcal{L} = & \bar{\psi}_i (i\partial - M) \psi_i + \frac{1}{2} \partial_\mu \sigma \partial^\mu \sigma - U(\sigma) - g_\sigma \bar{\psi}_i \sigma \psi_i \\
& - \frac{1}{4} \Omega_{\mu\nu} \Omega^{\mu\nu} + \frac{1}{2} m_\omega^2 \omega_\mu \omega^\mu - g_\omega \bar{\psi}_i \boldsymbol{\gamma} \boldsymbol{\omega} \psi_i \\
& - \frac{1}{4} \vec{R}_{\mu\nu} \vec{R}^{\mu\nu} + \frac{1}{2} m_\rho^2 \vec{\rho}_\mu \vec{\rho}^\mu - g_\rho \bar{\psi}_i \vec{\gamma} \vec{\rho} \psi_i \\
& - \frac{1}{4} F_{\mu\nu} F^{\mu\nu} - e \bar{\psi}_i \frac{1 - \tau_3}{2} \mathbf{A} \psi_i,
\end{aligned} \quad (1)$$

where  $\bar{\psi} = \psi^\dagger \gamma^0$  and  $\psi$  is the Dirac spinor. Other symbols have their usual meanings.

The Dirac equation for the nucleons and the Klein-Gordon type equations for the mesons and the photon are given by the variational principle and can be solved by expanding the wavefunctions in terms of the eigenfunctions of a deformed axially symmetric harmonic-oscillator potential [13] or a Woods-Saxon potential[14]. The details can be also found in Ref. [9] and references therein.

The potential energy curve can be calculated microscopically by the constrained RMF theory. The binding energy at certain deformation value is obtained by constraining the quadrupole moment  $\langle Q_2 \rangle$  to a given value  $\mu_2$  in the expectation value of the Hamiltonian [15],

$$\langle H' \rangle = \langle H \rangle + \frac{1}{2} C_\mu (\langle Q_2 \rangle - \mu_2)^2, \quad (2)$$

where  $C_\mu$  is the constraint multiplier.

For the nuclei studied in this paper, the full  $N = 20$  deformed harmonic oscillator shells are taken into account and the convergence of the numerical calculation on the

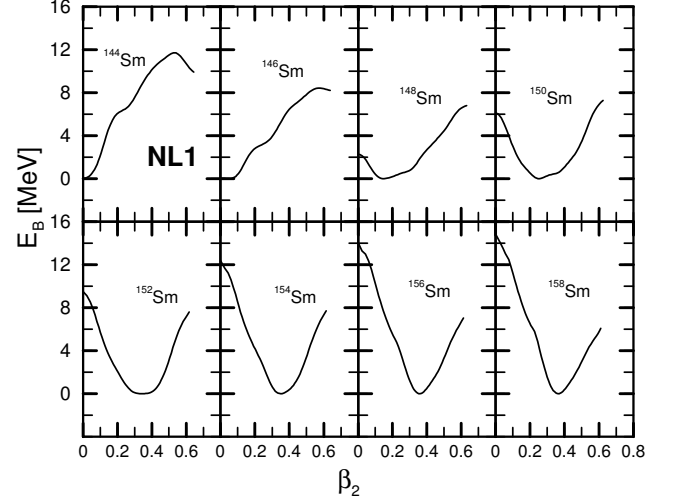


FIG. 1: The potential energy curves for  $^{144-158}\text{Sm}$  obtained by the constrained RMF theory with the NL1 parameter set. The ground state binding energy is taken as a reference.

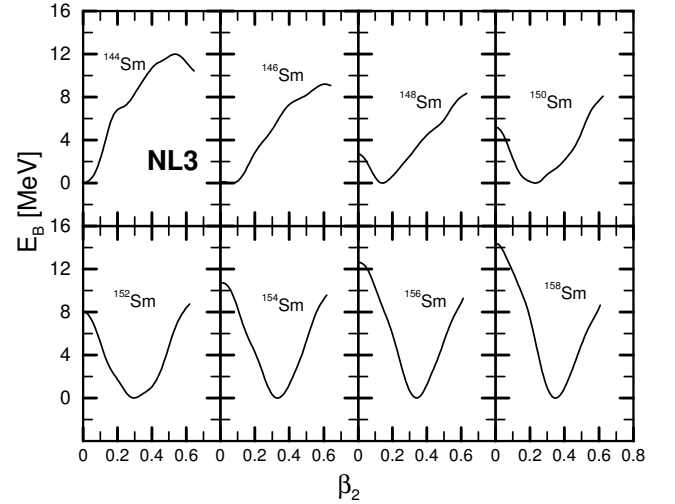


FIG. 2: The same as Fig. 1, but with NL3

binding energy and the deformation is very good. The converged deformations corresponding to different  $\mu_2$  are not sensitive to the deformation parameter  $\beta_0$  of the harmonic oscillator basis in a reasonable range due to the large basis. The different choices of  $\beta_0$  lead to different iteration numbers of the self-consistent calculation and different computational time. But physical quantities such as the binding energy and the deformation change very little. Thus the deformation parameter  $\beta_0$  of the harmonic oscillator basis is chosen near the expected deformation to obtain high accuracy and low computation time cost. By varying  $\mu_2$ , the binding energy at different deformation can be obtained. The pairing is considered by the constant gap approximation (BCS) in which the pairing gap is taken as  $\frac{12}{\sqrt{A}}$  for even number nucleons.

The binding energies and the quadrupole deforma-

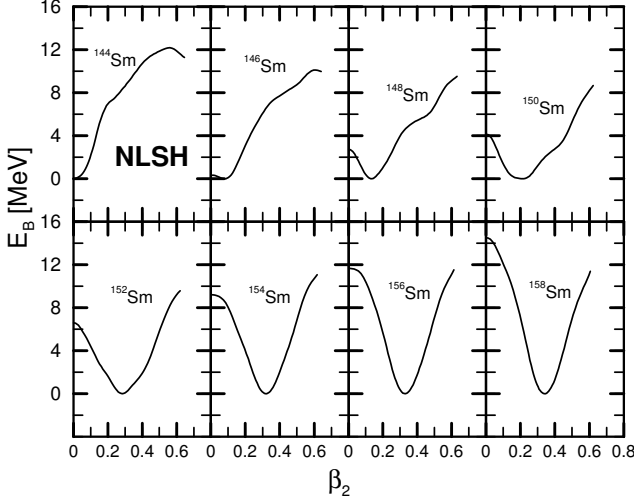


FIG. 3: The same as fig. 1, but with NLSH

tion for the ground states are listed in Table I in constrained RMF theory with NL1[16], NLSH[17], TM1[18] and NL3[19] parameter sets. For the binding energies, the data are well reproduced within 0.5 %. Particularly for NL3, excellent agreement (within 1 MeV) is observed for the binding energy in  $^{146-158}\text{Sm}$ . Even for neutron magic nuclei  $^{144}\text{Sm}$ , the difference between the RMF calculation and the data is less than 3 MeV, i.e., relatively less than 0.3 %. The spherical shapes in  $^{144,146}\text{Sm}$  and the weakly deformed  $^{148}\text{Sm}$  are well reproduced. The deformations in  $^{150-158}\text{Sm}$  are a little over-estimated by the theoretical calculations. In general, it can be concluded that the data is well reproduced by the constrained RMF theory.

Figures 1, 2, 3, and 4 show the potential energy curves for  $^{144-158}\text{Sm}$  in constrained RMF theory with NL1, NL3, NLSH and TM1 parameters, in which the energy for the ground state is taken as a reference. Similar patterns are found for all the parameter sets. The ground state of  $^{144}\text{Sm}$  is found to be spherical and has about 12 MeV stiff barrier against deformation. Although the ground state of  $^{146}\text{Sm}$  is still spherical, its barrier becomes around 8 MeV against deformation. With the increase of the neutron number, the ground state gradually moves toward the deformed side and the potential energy curve becomes more soft. Finally well deformed  $^{154-158}\text{Sm}$  are observed.

To examine how the shape of the Sm isotopes changes with the neutron number, the differences of the binding energy between the ground state and the state with spherical shape for Sm isotopes are presented in Table II in the constrained RMF theory with the NL1, NL3, NLSH and TM1 parameter sets. These differences can tell us how soft the nucleus is against deformation and may give us a hint on the phase transition of the nuclear shape. From  $^{144-158}\text{Sm}$ , the energy differences between the ground state and the state with spherical

TABLE II: The difference of the binding energy between the spherical state and the ground state in unit of MeV calculated by the constrained RMF theory with the NL1, NL3, NLSH and TM1 parameter sets for  $^{144-158}\text{Sm}$ .

	NL1	NL3	NLSH	TM1
$^{144}\text{Sm}$	0.00	0.00	0.00	0.00
$^{146}\text{Sm}$	0.02	0.11	0.33	0.07
$^{148}\text{Sm}$	2.26	2.67	2.72	1.98
$^{150}\text{Sm}$	6.11	5.19	4.13	3.08
$^{152}\text{Sm}$	9.51	8.02	6.59	3.38
$^{154}\text{Sm}$	12.33	10.73	9.20	4.37
$^{156}\text{Sm}$	14.10	12.61	11.64	6.53
$^{158}\text{Sm}$	14.80	14.36	14.51	8.68

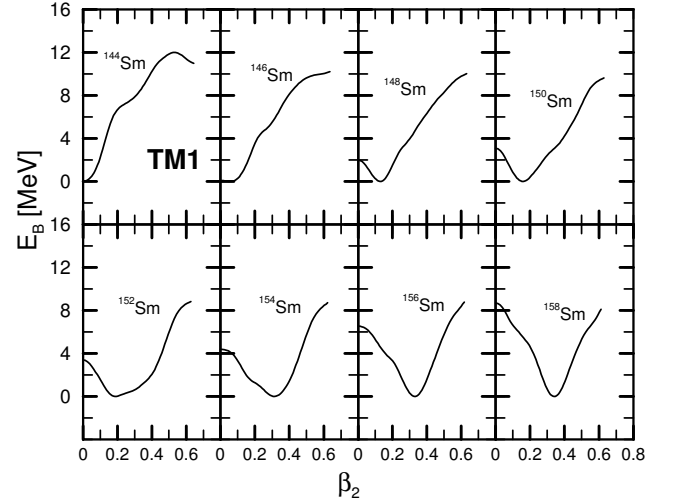


FIG. 4: The same as Fig. 1, but with TM1

shape change from 0 to 15 MeV. There are two jumps in the energy differences. The first jump appears at  $^{148}\text{Sm}$  and the second at  $^{154}\text{Sm}$ , which suggests the shape transition from spherical to critical point nuclei, and finally to axially deformed nuclei. The potential energy curves for  $^{148}\text{Sm}$ ,  $^{150}\text{Sm}$ , and  $^{152}\text{Sm}$  are relatively flat, i.e., they are  $\beta_2$ -soft nuclei in the transition between spherical and axially symmetric deformed nuclei.

One of the merits of microscopic nuclear models such as RMF theory is that it can provide detailed information on single particle levels, shell structure etc., which are very important for us to discuss nuclear structure and examine the deformation driving effect. In Fig. 5 the single neutron levels for  $^{144-158}\text{Sm}$  lying between 0 and -15 MeV are shown. The Fermi levels are presented by dashed line. Fig. 6 is similar to Fig. 5 but for protons. These two figures present results calculated with the parameter set TM1. The other three parameter sets give similar single particle structure thus not presented here.

From Figs. 5 and 6 one finds a consistency between the shell structure evolution and the shape evolution in Sm

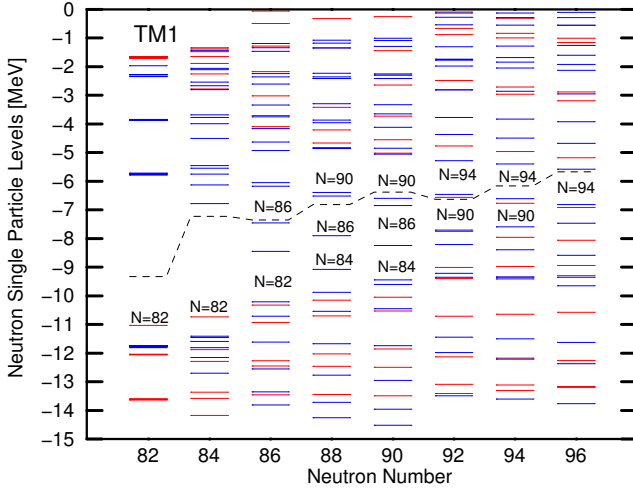


FIG. 5: The single neutron levels for  $^{144-158}\text{Sm}$  obtained by the constrained RMF theory with the TM1 parameter set.

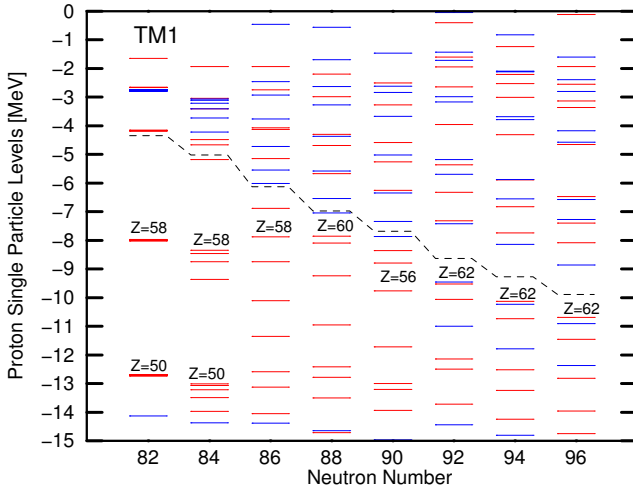


FIG. 6: The single proton levels for  $^{144-158}\text{Sm}$  obtained by the constrained RMF theory with the TM1 parameter set.

isotopes with increasing neutron number. Namely, for  $^{144}\text{Sm}$ , spherical symmetry is better restored. The deformation develops with  $N$  increasing. The deformation in  $^{146}\text{Sm}$  is still small and the energy gap with  $N = 82$  can be clearly seen from the single particle spectra. The nuclei  $^{148-150}\text{Sm}$  belong to a transition area, in which the  $N = 82$  gaps still exist but much smaller than that in  $^{144,146}\text{Sm}$ . Starting from  $^{154}\text{Sm}$ , the gap with  $N = 82$  disappears. Meanwhile a deformed gap for  $Z = 62$  develops and also that for  $N = 94$ . Correspondingly, we observe the well deformed  $^{154-158}\text{Sm}$ .

In summary, the shape transition between spherical and axially deformed nuclei in  $^{144-158}\text{Sm}$  are investigated by the microscopic quadrupole constrained relativistic mean field theory with all the most used interactions,

i.e., NL1, NL3, NLSH and TM1. The RMF calculation reproduces very well the data of the binding energy and deformation for the ground states. By examining the potential energy curves and the single particle levels obtained by this microscopic approach,  $^{148}\text{Sm}$ ,  $^{150}\text{Sm}$ , and  $^{152}\text{Sm}$  are found to be soft against  $\beta$  deformation and the critical point candidate nuclei, which marks the first order phase transition between spherical U(5) and axially deformed shapes SU(3).

We thank Victor Zamfir for helpful discussions and useful comments. This work was partly supported by the Major State Basic Research Development Program Under Contract Number G2000077407 and the National Natural Science Foundation of China under Grant No. 10025522, 10221003 and 10047001.

\* Electronic address: mengj@pku.edu.cn

- [1] F. Iachello and A. Arima, *The Interacting Boson Model* (Cambridge University Press, Cambridge, England, 1987).
- [2] A.E.L. Dieperink, O. Scholten, and F. Iachello, Phys. Rev. Lett. **44**, 1747 (1980).
- [3] D.H. Feng, R. Gilmore and S.R. Deans, Phys. Rev. **C23**, 1254 (1981).
- [4] F. Iachello, N.V. Zamfir, and F. Iachello, Phys. Rev. Lett. **81**, 1191 (1998).
- [5] F. Iachello, Phys. Rev. Lett. **87**, 052502 (2001).
- [6] R.F. Casten and N.V. Zamfir, Phys. Rev. Lett. **87**, 052503 (2001).
- [7] M.A. Caprio et al., Phys. Rev. C **66**, 054310 (2002).
- [8] B. Serot and J.D. Walecka, Adv. Nucl. Phys. **16**, 1 (1986).
- [9] P. Ring, Prog. Part. Nucl. Phys. **37**, 193 (1996).
- [10] J. Meng and P. Ring, Phys. Rev. Lett. **77**, 3963 (1996).
- [11] J. Meng, Nucl. Phys. **A 635**, 3 (1998).
- [12] J. Meng and P. Ring, Phys. Rev. Lett. **80**, 460 (1998).
- [13] Y. Gambhir, P. Ring, A. Thimet, Ann. Phys. (N.Y.) **198**, 132 (1990).
- [14] S.G.Zhou, J.Meng, P.Ring, Phys. Rev. C **68** (2003) 034323
- [15] P. Ring and P. Schuck, *The Nuclear Many Body Problem*, (Springer 1980).
- [16] P.G. Reinhard, M. Rufa, J. Maruhn, W. Greiner, and J. Friedrich, Z. Phys. A **323**, 13(1986).
- [17] M.M. Sharma, M.A. Nagarajan, and P. Ring, Phys. Lett. **B312**,377 (1993).
- [18] Y. Sugahara, and H. Toki, Nucl. Phys. **A 579**, 557 (1994).
- [19] G. A. Lalazissis, J. König, and P. Ring, Phys. Rev. **C55**, 540 (1997).
- [20] G. Audi, O. Bersillon and J. Blachot, Nucl. Phys. **A 624**, 1 (1997).
- [21] P. Möller, J. R. Nix, and W.D. Meyer, At. Data Nucl. Data Tables **59**, 1 (1995).